J. Fluid Mech. (2018), *vol.* 853, *pp.* 587–600.
doi:10.1017/jfm.2018.634

Hydrodynamic schooling of multiple self-propelled flapping plates

Ze-Rui Peng[1], **Haibo Huang**[1] **and Xi-Yun Lu**[1,†]

[1]Department of Modern Mechanics, University of Science and Technology of China, Hefei, Anhui 230026, PR China

(Received 22 February 2018; revised 19 June 2018; accepted 1 August 2018; first published online 29 August 2018)

While hydrodynamic interactions for aggregates of swimmers have received significant attention in the low Reynolds number realm ($Re \ll 1$), there has been far less work at higher Reynolds numbers, in which fluid and body inertia are involved. Here we study the collective behaviour of multiple self-propelled plates in tandem configurations, which are driven by harmonic flapping motions of identical frequency and amplitude. Both fast modes with compact configurations and slow modes with sparse configurations were observed. The Lighthill conjecture that orderly configurations may emerge passively from hydrodynamic interactions was verified on a larger scale with up to eight plates. The whole group may consist of subgroups and individuals with regular separations. Hydrodynamic forces experienced by the plates near their multiple equilibrium locations are all springlike restoring forces, which stabilize the orderly formation and maintain group cohesion. For the cruising speed of the whole group, the leading subgroup or individual plays the role of 'leading goose'.

Key words: biological fluid dynamics, propulsion, swimming/flying

1. Introduction

Collective behaviours are ubiquitous in biological and natural systems with large numbers of individuals acting with or being influenced by other individuals (Vicsek & Zafeiris 2012). Of particular interest are collections of actively moving bodies in a fluid where the flow-mediated interaction plays a crucial role. Biological examples include active collective locomotion with low Reynolds number ($Re \ll 1$), e.g. swimming micro-organisms (Saintillan & Shelley 2008; Lauga & Powers 2009; Zhang *et al.* 2010) and animal collectives with $Re \sim 10^2$–10^6, such as insect swarms (Kelley & Ouellette 2013), fish schools (Weihs 1973) and bird flocks (Portugal *et al.* 2014), in which the long-lasting inertial effects lead to more complex flows (Ramananarivo *et al.* 2016).

For the animal collectives, considerable attention has been paid to the social traits of collective behaviours, such as foraging, reproduction, and defence from predators (Parrish & Edelstein-Keshet 1999; Couzin *et al.* 2005). However, several issues about the role of hydrodynamics in collective locomotion are still open questions.

† Email address for correspondence: xlu@ustc.edu.cn

One important and intriguing issue is the role of flows on the emergence of the collective pattern. The fluid dynamicist Lighthill (1975) once conjectured that the orderly patterns could arise spontaneously as a consequence of passive flow-mediated interactions, without the need for 'elaborate control mechanisms'. This hypothesis, which is referred to as the 'Lighthill conjecture', has never been tested for groups on a larger scale (Zhu, He & Zhang 2014; Ramananarivo *et al.* 2016). The other issue concerns the hydrodynamic advantage. It is plausible that the individuals in collective locomotion are energy efficient due to favourable flow interactions that occur in specific formations (Weihs 1973; Portugal *et al.* 2014). However, quantitative information is limited because it is difficult to measure in experiments.

Because the two-body system is the simplest individual-level model, two passively flapping bodies (Ristroph & Zhang 2008; Alben 2009) and actively flapping flags or hydrofoils (Boschitsch, Dewey & Smits 2014; Uddin, Huang & Sung 2015) were studied to investigate their collective behaviour. However, in these studies the individuals were held fixed in the flow. A more realistic self-propelled model for an actively moving body was developed for further study (Alben & Shelley 2005; Hua, Zhu & Lu 2013). Recently the hydrodynamic behaviour of two self-propelled flapping filaments was studied numerically (Zhu *et al.* 2014). The results show that multiple stable tandem configurations can be formed passively from vortex-body interactions (Zhu *et al.* 2014). The 'vortex locking' mechanism was proposed, i.e., stable configurations can be spontaneously formed by locking the trajectories onto the vortex centres (Zhu *et al.* 2014).

Moreover, the collective locomotion dynamics of two flapping wings swimming in a tandem array was also studied experimentally (Becker *et al.* 2015; Ramananarivo *et al.* 2016). Becker *et al.* (2015) have shown that arrays of flapping and self-propelled wings select slow or fast modes due to constructive or destructive wing–wake interactions, respectively. In the study, they chose a periodic boundary condition horizontally, which implicitly means that there exist infinite plate interactions. In this way, each wing swims within the wakes of others. However, the horizontal spacing between the two plates was fixed so the configuration was imposed in the study of Becker *et al.* (2015). Hence, the set-up and physical mechanism are significantly different from that in Zhu *et al.* (2014). Ramananarivo *et al.* (2016) have shown that for two flapping plates, collective locomotion at enhanced speed and in orderly formations can emerge from flow interactions alone. Direct measurements of hydrodynamic forces acting on the follower reveal springlike restoring forces that maintain group cohesion (Ramananarivo *et al.* 2016). The idea of a hydrodynamic potential is also introduced in the study of Ramananarivo *et al.* (2016). It is a useful tool which we adopted here to analyse schooling stability. They noted a speed increase for pairs relative to a single body, indicating an influence on the leader by the follower. When the gap spacing is large, lack of flow feedback to the leading wing from the follower makes it effectively an isolated swimmer (Ramananarivo *et al.* 2016). To some extent, these studies support the perspective of the Lighthill conjecture for the two-body system. However, it is still unknown whether and to what extent the Lighthill conjecture is valid for a larger group.

To further verify the Lighthill conjecture, here we numerically investigate the hydrodynamic schooling of multi-body self-propelled systems consisting of flexible flapping plates. Self-propulsion is induced by the prescribed heave motion at the leading edge of each plate but whose longitudinal swimming is free. Two orderly schooling states are identified. The hydrodynamic interaction is analysed to reveal the mechanism. In addition, the schooling performances of the two states, including the cruising speed and swimming efficiency, are also discussed.

The remainder of this paper is organized as follows. The physical problem and mathematical formulation are presented in § 2. The numerical method and validation are described in § 3. Detailed results are discussed in § 4 and concluding remarks are addressed in § 5.

2. Physical problem and mathematical formulation

Here a self-propelled system consisting of N flapping flexible plates in a tandem configuration (see figure 1*a*) is investigated. Plates with identical length L are immersed in an initially stationary viscous incompressible fluid. The leading edges of the plates are forced to heave sinusoidally and in phase with identical amplitude A and frequency f in the lateral direction. The forced vertical motions of the leading edges are prescribed by $y(t) = A\cos(2\pi ft)$ with zero active pitching angle. The longitudinal distance between the leading edges of plates i and j is denoted by $D_{i,j}$. $G_{i,i+1}$ denotes the longitudinal distance between the trailing edge of the plate and the leading edge of its following plate, i.e., $G_{i,i+1} = D_{i,i+1} - 1$. In all simulations, if not specified, initially the plates are equally spaced with $G_{i,i+1} = G_0$, where $i = 1, 2, \ldots N-1$.

In this system, the fluid flow is governed by the incompressible Navier–Stokes equations

$$\frac{\partial \boldsymbol{v}}{\partial t} + \boldsymbol{v}\cdot\nabla\boldsymbol{v} = -\frac{1}{\rho}\nabla p + \frac{\mu}{\rho}\nabla^2\boldsymbol{v} + \boldsymbol{f}_b, \tag{2.1}$$

$$\nabla\cdot\boldsymbol{v} = 0, \tag{2.2}$$

where $\boldsymbol{v}$ is the velocity, p the pressure, ρ the density of the fluid, μ the dynamic viscosity, and $\boldsymbol{f}_b$ the body force term. The deformation and motion of plates are described by the structural equation (Hua *et al.* 2013),

$$\rho_l\frac{\partial^2\boldsymbol{X}}{\partial t^2} - Eh\frac{\partial}{\partial s}\left[\left(1 - \left|\frac{\partial\boldsymbol{X}}{\partial s}\right|^{-1}\right)\frac{\partial\boldsymbol{X}}{\partial s}\right] + EI\frac{\partial^4\boldsymbol{X}}{\partial^4 s} = \boldsymbol{F}_s, \tag{2.3}$$

where s is the Lagrangian coordinate along the plates, $\boldsymbol{X}(s, t) = (X(s, t), Y(s, t))$ is the position vector of the plates, $\boldsymbol{F}_s$ is the Lagrangian force exerted on the plates by the surrounding fluid and ρ_l is the structural linear mass density. Eh and EI are the structural stretching and bending rigidity, respectively.

For the structural equation, the boundary condition at the leading edges of the plates is $-Eh(1 - |\partial\boldsymbol{X}/\partial s|^{-1})\partial X/\partial s + EI\partial^3 X/\partial^3 s = 0$, $Y(t) = y(t)$, $\partial\boldsymbol{X}/\partial s = (1, 0)$, and the boundary condition at the free ends of the plates is $-Eh(1 - |\partial\boldsymbol{X}/\partial s|^{-1})\partial\boldsymbol{X}/\partial s + EI\partial^3\boldsymbol{X}/\partial^3 s = 0$, $\partial^2\boldsymbol{X}/\partial s^2 = 0$.

Following the scheme in Zou & He (1997), a constant pressure with $\boldsymbol{v} = 0$ is imposed at all boundaries except for the outlet. $\partial\boldsymbol{v}/\partial x = 0$ with the constant pressure imposed at the outlet (Zou & He 1997). At the initial time, the fluid velocity field is zero in the entire computational domain.

The characteristic quantities ρ, L and U_{ref} are chosen to normalize the above equations. Here, U_{ref} is the maximum flapping velocity of the plunging motion, i.e. $U_{ref} = 2\pi ALf$. The dimensionless governing parameters are described as follows: the Reynolds number $Re = \rho U_{ref}L/\mu$, the stretching stiffness $S = Eh/\rho U_{ref}^2 L$, the bending stiffness $K = EI/\rho U_{ref}^2 L^3$, the mass ratio of the plates and the fluid $M = \rho_l/\rho L$, the heaving amplitude A, the number of group member N, and the initial gap spacing G_0.

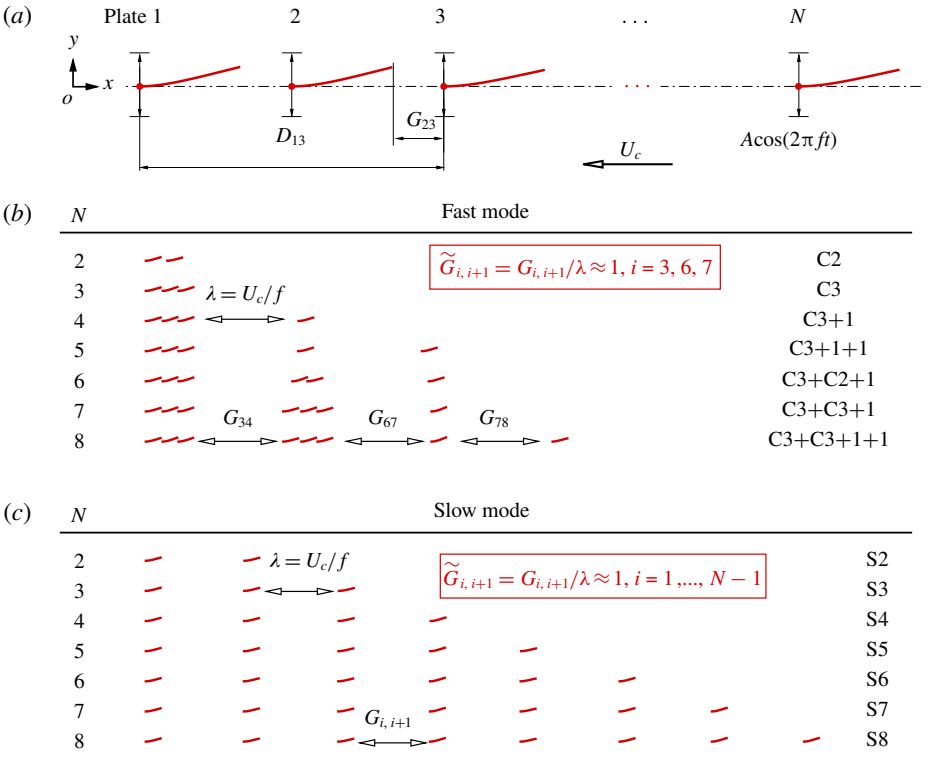

FIGURE 1. (Colour online) (*a*) Schematic diagram for the multi-body self-propelled system consisting of N flapping flexible plates in a tandem configuration. The longitudinal distance D, gap distance G and flapping amplitude A have been normalized by the dimensional length of the plate L. Snapshots of the orderly configurations for (*b*) the fast mode and (*c*) the slow mode. The notations 'C' and 'S' represent compact and sparse configurations, respectively. The number just following the notation denotes the number of plates in the subgroup (if any) or the group. For example, 'C3+C2+1' represents 3, 2 and 1 plates in the first, second and third subgroups in the compact configuration, respectively.

3. Numerical method and validation

The Navier–Stokes equations are solved numerically by the lattice Boltzmann method (LBM) (Chen & Doolen 1998). The deformation and motion of each plate are described by a structural equation, i.e., equation (2.3). Each structural equation is solved by a finite element method in the Lagrange coordinate independently (Doyle 2001). For each plate, boundary conditions for the leading and trailing ends are imposed. The movement of each plate (Lagrange points) is coupled with the LBM solver through immersed boundary methods (Peskin 2002; Mittal & Iaccarino 2005). The body force term $\boldsymbol{f}_b$ in (2.1) represents an interaction force between the fluid and the immersed boundary to enforce the no-slip velocity boundary condition. A detailed description of the numerical method can be found elsewhere (Hua *et al.* 2013; Hua, Zhu & Lu 2014).

Based on our convergence studies with different computational domains, the computational domain for fluid flow is chosen as $(D_{1N} + 50)L \times 40L$ in the x

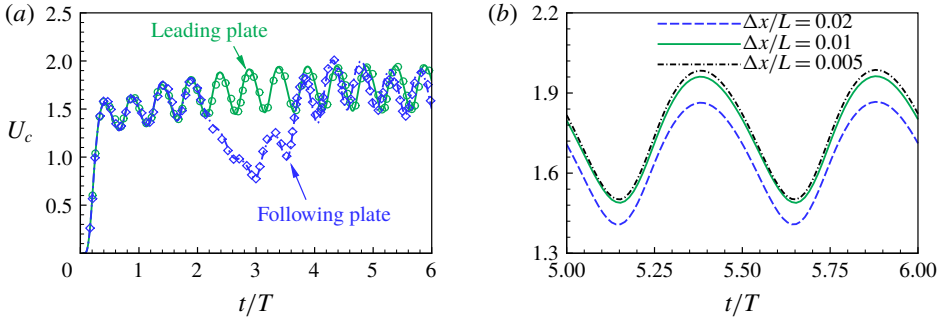

FIGURE 2. (Colour online) (*a*) Numerical validation. Lines and symbols represent the present results and those in Zhu *et al.* (2014), respectively. (*b*) Grid-independence study. A case of two self-propelled plates in a tandem configuration is simulated. In the case, the key parameters, $Re = 200$, $A = 0.5$, $M = 0.2$, $K = 0.8$, $S = 1000$ and $G_0 = 8.0$, are identical to those in Zhu *et al.* (2014). U_c is the cruising speed.

and y directions. The domain is large enough so that the blocking effects of the boundaries are not significant.

In the x and y directions, the mesh is uniform with spacing $\Delta x = \Delta y = 0.01L$. The time step is $\Delta t = T/10\,000$ for the simulations of fluid flow and plate deformation, with $T = 1/f$ being the flapping period. Moreover, a finite moving computational domain (Hua *et al.* 2013) is used in the x direction to allow the plates to move for a sufficiently long time. As the plate travels one lattice spacing in the x direction, the computational domain is shifted, i.e. one layer being added at the inlet and another layer being removed at the outlet (Hua *et al.* 2013).

To validate the present numerical method, the coupling locomotion of two self-propelled plates in a tandem configuration is simulated. Figure 2(*a*) shows the cruising speeds of the leading and following plates as a function of time. It is seen that the present results agree well with those of Zhu *et al.* (2014). Moreover, the cruising speeds of the leading plate obtained from different grid resolutions are shown in figure 2(*b*). It is seen that $\Delta x/L = 0.01$ is sufficient to achieve accurate results. In addition, the numerical strategy used in this study has been validated and successfully applied to a wide range of flows, such as the dynamics of fluid flow over a circular flexible plate (Hua *et al.* 2014) and the locomotion of a flapping flexible plate (Hua *et al.* 2013).

4. Results and discussion

In our simulations, the typical non-dimensional parameters are: $Re = 200$, $A = 0.5$, $M = 0.2$, $S = 1000$ and $K = 1$. Here, the stretching stiffness of plate is chosen to be large enough ($S = 1000$) so that the stretching deformation is negligible. Usually the bending stiffness K of a fish is $O(1)$; for example, the tail fin of a goldfish (*Carassius auratus*) has a bending stiffness of $2.5 \sim 23$ (Hua *et al.* 2013). (It is noted that the characteristic velocities are $U_{ref} = 2\pi ALf$ and $U_{ref} = Lf$ in the present study and Hua *et al.* (2013), respectively.) In our study K is fixed to be unity. At $M = 0.2$, an isolated plate with $K = 1$ achieves the maximum cruising speed. These parameters are also consistent with those in Zhu *et al.* (2014). In our study, $N \in [2, 8]$, $G_0 \in (0, 6]$; they are variable.

4.1. *Schooling states*

The cruising speed of the ith plate is defined as the averaged forward speed at the equilibrium state, i.e. $U_{c,i} = \int_0^T u_i(t)\,\mathrm{d}t/T = \int_0^T |\partial_t X_i(0,\,t)|\,\mathrm{d}t/T$, where $u_i(t)$ is the instantaneous speed of the ith plate. At the equilibrium state, the cruising speed of the whole group is $U_c = U_{c,i},\ i = 1, 2, \ldots N$.

Results of our simulations show that two distinct stable schooling states emerge spontaneously. According to U_c, they are classified as the fast and slow modes. Figures 1(*b*) and 1(*c*) show snapshots of the configurations for the two modes, respectively. It is seen that the two modes can also be identified according to the spatial configuration of the plates. The emergence of distinct orderly formations depends on G_0. In particular, the compact and sparse configurations appear when $G_0 \leqslant 2.3$ and $2.5 \leqslant G_0 \leqslant 6$, respectively. For the effect of the initial gap spacing G_0, we can imagine that if G_0 is large enough, the interactions between plates are negligible and the plates flap and move independently. Hence we do not intend to investigate cases with too large G_0, and limit the present study to the range $G_0 \leqslant 6$.

For the fast mode, as the group size increases, the group may spontaneously split into several subgroups or individuals. Each subgroup in the compact mode consists of up to three members (see figure 1*b*). For the slow mode with a sparse configuration, when $G_0 \geqslant 5$, at the equilibrium state the gap spacings between any two neighbouring plates are identical and subgroups are not observed, as shown in figure 1(*c*). For corresponding flow fields, please refer to the supplementary movies available at https://doi.org/10.1017/jfm.2018.634. Typical cases of the fast mode 'C3+1' and 'C3+C2+1' are shown in Movies 1 and 2, respectively. Typical cases of the slow mode 'S4', 'S6', 'S6+S2', and 'S8' are shown in Movies 3–6, respectively. The notations 'C' and 'S' represent compact and sparse configurations, respectively. The number just following the notation denotes the number of plates in the subgroup (if any) or the group.

To quantitatively describe the evolution of the orderly formations, two typical cases with $N = 8$, $G_0 = 1$ and $N = 8$, $G_0 = 5$ are taken as examples. The locations of the following plates (i.e. $i = 2, \ldots, N$) described by D_{1i} as a function of time for the two cases are shown in figures 3(*a*,*b*). It is seen that when $t > 15T$, all distances D_{1i} reach equilibrium states in both cases. The cases $G_0 = 1$ and $G_0 = 5$ evolve to two distinct equilibrium states: the compact ('C3+C3+1+1') and sparse ('S8') configurations, respectively.

The schooling number introduced by Becker *et al.* (2015) has been used to quantify collective patterns of the two-wing system (Becker *et al.* 2015; Ramananarivo *et al.* 2016). Here it is defined as $\widetilde{G}_{i,i+1} = G_{i,i+1}/\lambda$, where $\lambda = U_c/f$ is the wavelength. In the fast mode, the schooling numbers within the compact subgroups, such as $\widetilde{G}_{12}$ and $\widetilde{G}_{23}$, approximately converge to zero, whereas the inter-subgroup schooling numbers, such as $\widetilde{G}_{34}$ and $\widetilde{G}_{67}$, approximately approach unity (see figure 1*b* 'C3+C3+1+1'). In the slow mode illustrated in figure 1(*c*), the inter-individual schooling numbers are also close to unity.

Figures 3(*c*) and 3(*d*) show the schooling numbers of the fast and slow modes, respectively. In the fast mode, the inter-individual spacings within the compact subgroups, such as $\widetilde{G}_{12}$ and $\widetilde{G}_{23}$ in figure 3(*a*), approximately converge to zero, whereas the inter-subgroup schooling numbers, such as $\widetilde{G}_{34}$ and $\widetilde{G}_{67}$, approximately approach unity. In the slow mode, the inter-individual schooling numbers within the group are identical, i.e. $\widetilde{G}_{i,i+1} = 1,\ i = 1, 2, \ldots, 7$.

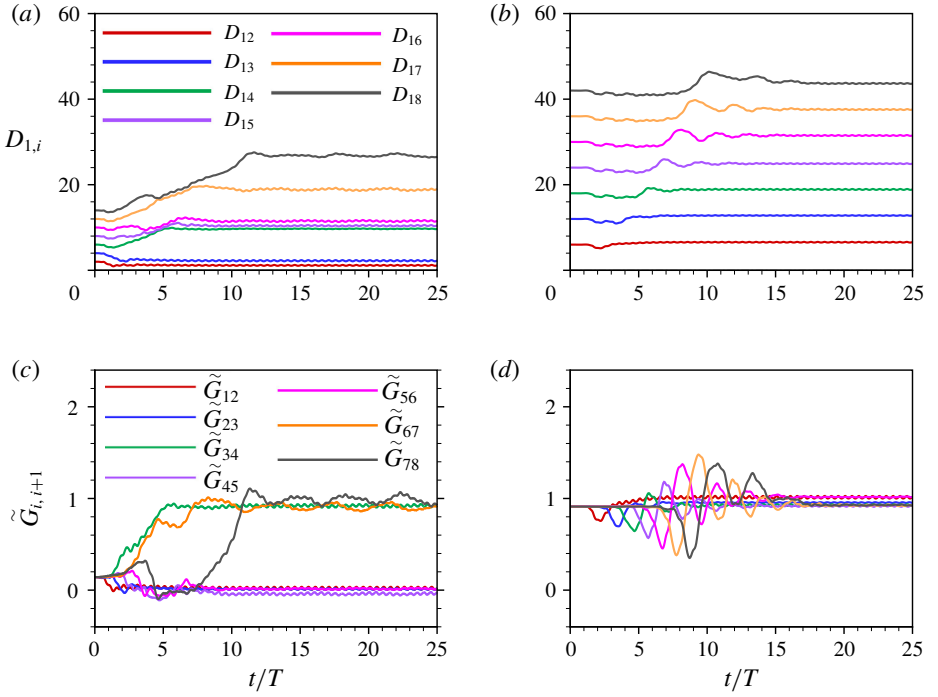

FIGURE 3. (Colour online) Dynamics of the orderly formations. (*a*,*b*) The distances between the following plates and the leading plate, i.e., $D_{1,i}$ ($i = 2, \ldots, N$) and (*c*,*d*) the schooling number as a function of time. (*a*,*c*) Case 'C3+C3+1+1'. (*b*,*d*) Case 'S8'. In both cases $N = 8$.

Case	Fast mode				Slow mode	Isolated plate
	C2	C3	C4	C5		
U_c	2.09	2.24	2.35	2.41	1.75	1.75

TABLE 1. The cruising speed U_c of groups with leading compact subgroups 'Cn', $n = 2$, 3, 4 and 5. The results of the slow mode and the isolated plate are also presented.

For the fast mode, the maximum number of members in the compact subgroup, n, does not always have to be three. It depends on the initial gap spacing. For the case $N = 4$ with uniform gap spacing $G_0 = 1$, 'C3+1' would appear (see figure 4*a*). When the initial gap spacing is non-uniform (see the caption of figure 4), the fast mode with a leading subgroup consisting of four or five plates would also emerge. In figure 4(*b*,*c*), the instantaneous vorticity structures at equilibrium states for cases 'C4+1' and 'C5+1' are shown. The schooling number $\widetilde{G} = G/\lambda$ is found to be unity for all three cases in figure 4, where G is the gap distance between the additional plate '1' and its front neighbour. It indicates that there is similar hydrodynamic mechanism in the fast mode with compact configurations, which is not dependent on n. The cruising speed of the leading compact subgroups is listed in table 1. It is seen that the larger n is, the faster the whole group travels. A possible reason is that the compact plates in a subgroup act as a longer plate, which has a larger U_c (Rosellini & Zhang 2007).

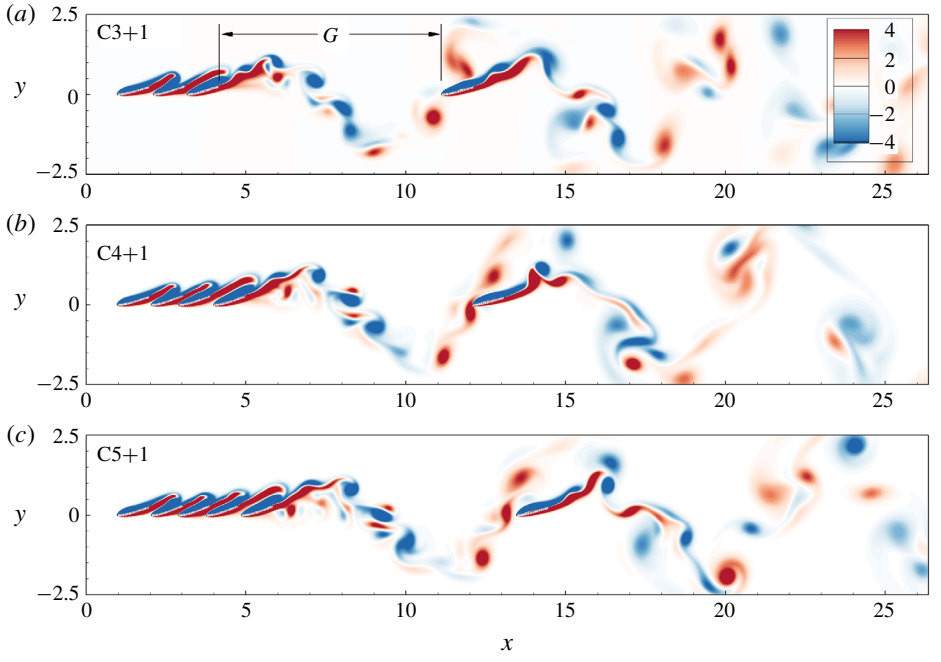

FIGURE 4. (Colour online) Formation of 'C4' and 'C5' in the compact configurations. Typical instantaneous vorticity structures of the compact configurations at $t/T = 1/4$: (a) case 'C3+1' with the uniform initial separation $G_0 = 1$, (b) case 'C4+1' with $G_{i,i+1}(t = 0) = 1$ ($i = 1, 2, 3$) and $G_{45}(t = 0) = 0.5$, and (c) case 'C5+1' with $G_{i,i+1}(t = 0) = 1$ ($i = 1, 2, 3, 4$) and $G_{56}(t = 0) = 0.5$.

It is worth noting that for the slow mode, the group may also split, which depends on the initial configuration. For example, when the initial gap distance $G_0 = 3$, the stable formation consisting of two subgroups is observed. It is referred to as 'S6+S2' (see Movie 5). The front and rear subgroups contain six and two plates, respectively. The gap spacings within the subgroups are uniform, e.g. $\widetilde{G}_{i,i+1} = 1$ ($i = 1, 2, \ldots, 5$ and 7), and the inter-subgroup spacing is $\widetilde{G}_{67} = 2$.

4.2. *Schooling stability*

These stable and orderly formations with spontaneously selected integer values of schooling numbers are a result of long-range wake–plate interactions. The vorticity contours at $t/T = 1/4$ for the cases 'C3' and 'S6' are shown in figures 5(a) and 5(b), respectively. It is seen that the wakes of the 'C3' and 'S6' evolve from a chaotic and perturbed state to an orderly vortex street along the distance downstream through vorticity merging and dissipation. Suppose the case of 'C3' reaches a stable state as shown in figure 5(a); if an additional plate is inserted into the wake of 'C3', it would be 'locked' into several discrete equilibrium positions. Which equilibrium position it adopts depends on the initial gap spacing G_{34}. The circumstance of the case 'S6' is similar. The locations labelled by the up arrows approximately have integer schooling numbers, i.e. $\widetilde{G} \approx 1, 2, \ldots, 6$. This observation is consistent with that of the two-body system (Zhu *et al.* 2014; Ramananarivo *et al.* 2016), indicating that the additional

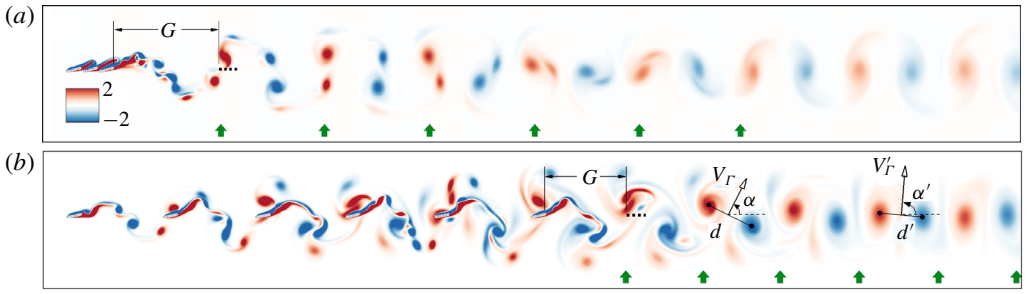

FIGURE 5. (Colour online) Instantaneous vorticity contours for the cases 'C3' (*a*) and 'S6' (*b*) at $t/T = 1/4$. If an additional plate (represented by the bold dashed line) is inserted into the wake, the six sequential equilibrium locations are marked with green up arrows near the x-axis. G is the gap distance between the additional plate and its front neighbour. α, α' are the orientation angles between the dipole-induced velocities V_Γ, V'_Γ and the x-axis. d and d' are distances between two vortex centres.

plates are able to keep pace with oncoming wake of the leading subgroup even though the flow perturbation increases compared to the two-body system.

To further explore the mechanism for the emergence of the equilibrium positions, the hydrodynamic forces on the additional or the trailing plate in the cases of 'C3' and 'S6' (see figure 5) are calculated. For convenience, the simulations were performed in an inertial coordinate system moving with velocity U_c in the negative x-direction. It is noted that before the simulations, the equilibrium states for cases of 'C3' and 'S6' and their U_c have been figured out. In the inertial frame, the oncoming flow has a uniform longitudinal velocity of U_c and the longitudinal locations of the plates are fixed to be those at the equilibrium state. Figure 6(*a*) shows the net horizontal force F_x acting on the trailing plate as a function of $\widetilde{G}$ for the cases 'C3+1' and 'S6+1'. It is seen that for both the modes, there are several discrete points with $F_x = 0$, such as $\widetilde{G} \approx 1$, 1.4, 2, 2.5, 3, ... However, only the points with negative $\mathrm{d}F_x/\mathrm{d}\widetilde{G}$ are stable, at which $\widetilde{G} \approx 1, 2, 3 \ldots$. The hydrodynamic force near the stable equilibrium positions is a springlike restoring force with $F_x \approx -k(\widetilde{G} - \widetilde{G}^{eq})$, where $\widetilde{G}^{eq}$ is the ith stable equilibrium location and $k = -\mathrm{d}F_x/\mathrm{d}\widetilde{G}$ is analogous to the spring constant. In addition, the emergence of equilibrium positions may be illustrated in terms of a hydrodynamic potential, which is defined as the integral of force with respect to distance, i.e. $\Psi(\widetilde{G}) = -\int F_x \,\mathrm{d}\widetilde{G}$. As shown in figure 6(*b*), there are stable wells in the potential energy landscape. The well bottoms correspond to the stable equilibrium states, at which $\widetilde{G}^{eq} \approx 1, 2, 3, 4$. The peak points are unstable equilibrium states which are not observed in the simulations.

To evaluate the tolerance for flow perturbation at the stable positions, the well depths in the curve of $\Psi(\widetilde{G})$, which are denoted by ξ^p, are measured. Figure 6(*c*) shows ξ^p as a function of stable position $\widetilde{G}^{eq}$ for the cases 'C3+1' and 'S6+1', as well as the slow mode for the two-plate system ('S2'). It is seen that for the case 'S2', ξ^p decreases with $\widetilde{G}^{eq}$, which is consistent with the experimental result in the two-body system (Ramananarivo *et al.* 2016). In contrast, for the larger groups, such as 'C3+1' and 'S6+1', ξ^p increases and then decreases with increasing $\widetilde{G}^{eq}$. In other words, for all equilibrium cases of 'C3+1', the case with the trailing plate at $\widetilde{G}^{eq} = 4$ is more stable than the cases of $\widetilde{G}^{eq} = 1$, 2, 3 and $\widetilde{G}^{eq} = 5$, 6. For the

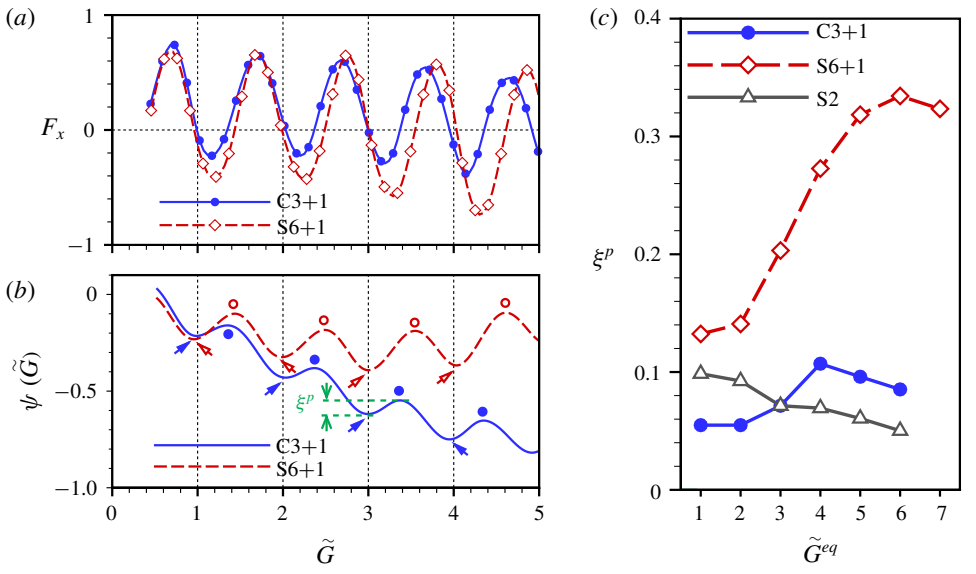

FIGURE 6. (Colour online) Hydrodynamic forces F_x (*a*) and potentials $\Psi(\widetilde{G}) = -\int F_x \,\mathrm{d}\widetilde{G}$ (*b*) as a function of $\widetilde{G}$, $\widetilde{G} = G/\lambda$. The valleys (well bottoms) and peaks of Ψ are marked with arrows and circles, showing the stable ($\widetilde{G}^{eq}$) and unstable equilibrium locations, respectively. Well depth ξ^p at $\widetilde{G}^{eq} = 3$ for the case 'C3+1' is shown as an example. (*c*) ξ^p as a function of $\widetilde{G}^{eq}$.

trailing plate in the wake of the leading subgroup, the stability around its equilibrium state is relevant to the vertical flow induced by the vortices. From figure 5(*b*), it is seen that α' is closer to 90° than α and d' is smaller than d, where α and α' are the orientation angles between the dipole-induced velocities V_Γ, V'_Γ and the x-axis, and d and d' are distances between two vortex centres. Although the vortex circulation Γ' at $\widetilde{G}^{eq} \approx 4$ is slightly smaller than Γ at $\widetilde{G}^{eq} \approx 2$, the vertical component of the dipole-induced velocity $V'_\Gamma \sin\alpha'$ at $\widetilde{G}^{eq} \approx 4$ is larger according to the vortex-dipole model $V'_\Gamma \sin\alpha' = (\Gamma'/2\pi d')\sin\alpha'$ (Godoy-Diana *et al.* 2009). It would result in an enhanced hydrodynamic restoring force at $\widetilde{G}^{eq} \approx 4$ (Wu & Chwang 1975; Ramananarivo *et al.* 2016) and therefore the value of ξ^p at $\widetilde{G}^{eq} = 4$ is enhanced compared to that at $\widetilde{G}^{eq} = 2$. On the other hand, when $\widetilde{G}^{eq}$ becomes larger, e.g. $\widetilde{G}^{eq} \geqslant 7$, ξ^p would decrease because the wake–plate interaction is diminished for the trailing plate due to vortex dissipation.

For the two-plate system, using the 'vortex locking' mechanism, Zhu *et al.* (2014) explained the energy benefit of the rear plate. Meanwhile, they also mentioned that if the rear plate slaloms between the vortex cores, it is not able to obtain the energy benefit. However, the mechanism is not true for the multiple plate system. From supplementary Movie 2, it is seen that in the 'C3+C2+1' configuration, the last plate ($i = 6$) moves forward by slaloming between the vortex cores, instead of swimming through the vortex cores. This slaloming behaviour is also beneficial to enhancing propulsive performance because the last plate moves approximately 1.3 times faster than an isolated plate. Moreover, because the wakes of a multi-body group may become disorganized as the group grows, the 'vortex locking' mechanism is also

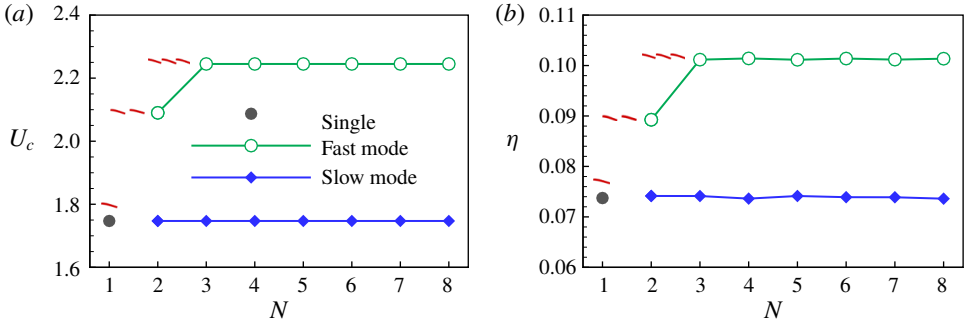

FIGURE 7. (Colour online) Schooling performance of the groups. (*a*) The cruising speed and (*b*) the swimming efficiency as a function of the group size N. Small snapshots of the leading subgroup or individual are shown in red.

not valid. Supplementary Movies 5 and 6 show that even encountering a disordered oncoming vortical structure, the last plate in case 'S8' is still able to hold its position in the stable configuration.

For the multiple plate system, the mechanism of 'hydrodynamic force generation by effective flapping speed' (Wu & Chwang 1975; Ramananarivo *et al.* 2016) seems more general and appropriate than 'vortex locking'. The mechanism states 'hydrodynamic force on the follower is due to the vorticity induced by the leader', specifically the thrust is mainly induced by 'effective wing flapping speed' (i.e., the relative vertical velocity of the wing and the fluid) (Ramananarivo *et al.* 2016). In the above discussion the mechanism is adopted to explain why the hydrodynamic restoring force at $\widetilde{G}^{eq} = 4$ is enhanced.

4.3. *Schooling performance*

To quantify the schooling performance of each plate, the swimming efficiency η_i is defined as the ratio of the kinetic energy of the ith plate and its input work, i.e. $\eta_i = (1/2)MU_{c,i}^2/W_i$, where the input work W_i is computed as a time integral of the input power P_i required to produce the oscillation and the forward movement (Hua *et al.* 2013; Zhu *et al.* 2014), i.e. $W_i = \int_0^T P_i(t)\,\mathrm{d}t = -\int_0^T \int_0^1 \boldsymbol{F}_{s,i}(s,t) \cdot \partial_t \boldsymbol{X}_i(s,t)\,\mathrm{d}s\,\mathrm{d}t$. The swimming efficiency of the whole group is

$$\eta = \frac{1}{2}M \sum_{i=1}^{N} U_{c,i}^2 \Bigg/ \sum_{i=1}^{N} W_i. \tag{4.1}$$

Figure 7(*a*,*b*) show the cruising speed and the swimming efficiency of the group as a function of N for the cases in figure 1(*b*,*c*). For the slow mode, the groups' cruising speeds and their efficiencies are almost identical to those of the isolated swimmer. In contrast, for the fast mode, the groups have larger U_c with higher η compared to the isolated case. For the groups with $N > 3$, $U_c \approx 2.24$ and $\eta \approx 0.10$, they are approximately 1.3 times those of the isolated plate, as shown in figure 7.

Moreover, it is interesting to see that the leading subgroup plays the role of 'leading goose'; namely, the following subgroups or individuals would keep pace with the leading ones to achieve a uniform cruising speed, although they may have different speeds in isolated swimming. Taking case 'C3+C2+1' (see figure 1) as an example, we

can see that if the subgroups 'C3', 'C2', and the individual '1' swim independently, the cruising speeds are 2.24, 2.09 and 1.75 (see table 1), respectively. However, when swimming together as a group, they achieve a uniform cruising speed $U_c = 2.24$, as shown in figure 7(*a*). Meanwhile, the swimming efficiency of the group members 'C2' and '1' is improved (see figure 7*b*). In the fast mode, following the leading packed subgroup, the rear subgroups or individuals take advantage of the oncoming wake. These conclusions indicate the hydrodynamic force not only acts as an restoring force to maintain schooling cohesion but also provides a drafting force to rear subgroups so as to improve their schooling performance.

5. Concluding remarks

In summary, the collective locomotion of multiple self-propelled plates in a tandem configuration is investigated numerically. Two schooling states, i.e., the fast mode with compact configuration and the slow mode with sparse configuration, emerge spontaneously solely due to the flow-mediated interactions among the individuals. The Lighthill conjecture (Lighthill 1975) was supported by the results of multiple self-propelled plates, which is beyond the cases of the two-body system considered elsewhere (Zhu *et al.* 2014; Ramananarivo *et al.* 2016).

Schooling stability analysis shows the mechanism for the emergence of the equilibrium positions. It is found that the hydrodynamic force near the stable equilibrium positions is a springlike restoring force. In addition, the emergence of equilibrium positions can be illustrated in terms of a hydrodynamic potential; there are stable wells in the potential energy landscape. The well bottoms correspond to the stable equilibrium states.

The well depths ξ^p in the curve of $\Psi(\widetilde{G})$ are examined to quantify the tolerance for flow perturbation at the stable positions. For the two-plate system, the well depth ξ^p decreases with increasing $\widetilde{G}^{eq}$, while for multiple plates, the well depth ξ^p may increase first and then decrease with $\widetilde{G}^{eq}$.

For the multiple plate system, the last plate may move forward by slaloming between the vortex cores, instead of swimming through the vortex cores. The 'vortex locking' mechanism (Zhu *et al.* 2014) is no longer valid. The mechanism of 'hydrodynamic force generation by effective flapping speed' (Wu & Chwang 1975; Ramananarivo *et al.* 2016) seems more general and appropriate.

For the slow mode, the groups' cruising speeds and their efficiencies are almost identical to those of the isolated swimmer. In contrast, for the fast mode, the groups have larger U_c with higher η compared to the isolated case. In terms of the cruising speed and efficiency of the whole group, the leading subgroup or individual plays the role of 'leading goose'. It seems that the hydrodynamic force also provides a drafting force to rear subgroups so as to improve their schooling performance.

The present study is a generalization of the two-plate system (Zhu *et al.* 2014) to more wings/flappers (up to $O(10)$) and the Lighthill conjecture is further validated on a larger scale. There are some limitations in our study. First, the present model is only two-dimensional, but extending it to the three-dimensional case would be helpful to examine the role of body shape. Second the actuation of the swimming is simple, i.e., only the leading edge of the plate is forced to oscillate sinusoidally. To mimic the actuation of a real fish, a better actuation model, e.g., the neuromechanical model for a lamprey (Tytell *et al.* 2010), should be applied rather than the simplified oscillation model here. If the three-dimensional body shape and a better actuation model are considered, the fish schooling behaviour revealed may be more reasonable.

Acknowledgements

This work was supported by the Natural Science Foundation of China (NSFC) grant nos 11372304 and 11621202. H.B.H. is supported by NSFC grant no. 11772326.

Supplementary movies

Supplementary movies are available at https://doi.org/10.1017/jfm.2018.634.

REFERENCES

ALBEN, S. 2009 Wake-mediated synchronization and drafting in coupled flags. *J. Fluid Mech.* **641**, 489–496.

ALBEN, S. & SHELLEY, M. J. 2005 Coherent locomotion as an attracting state for a free flapping body. *Proc. Natl Acad. Sci. USA* **102**, 11163–11166.

BECKER, A. D., MASOUD, H., NEWBOLT, J. W., SHELLEY, M. & RISTROPH, L. 2015 Hydrodynamic schooling of flapping swimmers. *Nat. Commun.* **6**, 8514.

BOSCHITSCH, B. M., DEWEY, P. A. & SMITS, A. J. 2014 Propulsive performance of unsteady tandem hydrofoils in an in-line configuration. *Phys. Fluids* **26**, 051901.

CHEN, S. & DOOLEN, G. D. 1998 Lattice Boltzmann method for fluid flows. *Annu. Rev. Fluid Mech.* **30**, 329–364.

COUZIN, I. D., KRAUSE, J., FRANKS, N. R. & LEVIN, S. A. 2005 Effective leadership and decision-making in animal groups on the move. *Nature* **433** (7025), 513–516.

DOYLE, J. F. 2001 *Nonlinear Analysis of Thin-Walled Structures: Statics, Dynamics, and Stability*. Springer.

GODOY-DIANA, R., MARAIS, C., AIDER, J.-L. & WESFREID, J.-E. 2009 A model for the symmetry breaking of the reverse Bénard–von Kármán vortex street produced by a flapping foil. *J. Fluid Mech.* **622**, 23–32.

HUA, R.-N., ZHU, L. & LU, X.-Y. 2013 Locomotion of a flapping flexible plate. *Phys. Fluids* **25**, 121901.

HUA, R.-N., ZHU, L. & LU, X.-Y. 2014 Dynamics of fluid flow over a circular flexible plate. *J. Fluid Mech.* **759**, 56–72.

KELLEY, D. H. & OUELLETTE, N. T. 2013 Emergent dynamics of laboratory insect swarms. *Sci. Rep.* **3**, 1073.

LAUGA, E. & POWERS, T. R. 2009 The hydrodynamics of swimming microorganisms. *Rep. Prog. Phys.* **72** (9), 096601.

LIGHTHILL, M. J. 1975 *Mathematical Biofluiddynamics*. SIAM.

MITTAL, R. & IACCARINO, G. 2005 Immersed boundary methods. *Annu. Rev. Fluid Mech.* **37**, 239–261.

PARRISH, J. K. & EDELSTEIN-KESHET, L. 1999 Complexity, pattern, and evolutionary trade-offs in animal aggregation. *Science* **284**, 99–101.

PESKIN, C. S. 2002 The immersed boundary method. *Acta Numerica* **11**, 479–517.

PORTUGAL, S. J., HUBEL, T. Y., FRITZ, J., HEESE, S., TROBE, D., VOELKL, B., HAILES, S., WILSON, A. M. & USHERWOOD, J. R. 2014 Upwash exploitation and downwash avoidance by flap phasing in ibis formation flight. *Nature* **505** (7483), 399–402.

RAMANANARIVO, S., FANG, F., OZA, A., ZHANG, J. & RISTROPH, L. 2016 Flow interactions lead to orderly formations of flapping wings in forward flight. *Phys. Rev. Fluids* **1** (7), 071201.

RISTROPH, L. & ZHANG, J. 2008 Anomalous hydrodynamic drafting of interacting flapping flags. *Phys. Rev. Lett.* **101** (19), 194502.

ROSELLINI, L. & ZHANG, J. 2007 The effect of geometry on the flapping flight of a simple wing. http://www.physics.nyu.edu/jz11/publications/LT10521stop.pdf.

SAINTILLAN, D. & SHELLEY, M. J. 2008 Instabilities and pattern formation in active particle suspensions: kinetic theory and continuum simulations. *Phys. Rev. Lett.* **100**, 178103.

TYTELL, E. D., HSU, C.-Y., WILLIAMS, T. L., COHEN, A. H. & FAUCI, L. J. 2010 Interactions between internal forces, body stiffness, and fluid environment in a neuromechanical model of lamprey swimming. *Proc. Natl Acad. Sci. USA* **107** (46), 19832–19837.

UDDIN, E., HUANG, W.-X. & SUNG, H. J. 2015 Actively flapping tandem flexible flags in a viscous flow. *J. Fluid Mech.* **780**, 120–142.

VICSEK, T. & ZAFEIRIS, A. 2012 Collective motion. *Phys. Rep.* **517** (3), 71–140.

WEIHS, D. 1973 Hydromechanics of fish schooling. *Nature* **241**, 290–291.

WU, T. Y. & CHWANG, A. T. 1975 Extraction of flow energy by fish and birds in a wavy stream. In *Swimming and Flying in Nature*, pp. 687–702. Springer.

ZHANG, H.-P., BEER, A., FLORIN, E.-L. & SWINNEY, H. 2010 Collective motion and density fluctuations in bacterial colonies. *Proc. Natl Acad. Sci. USA* **107**, 13626–13630.

ZHU, X., HE, G. & ZHANG, X. 2014 Flow-mediated interactions between two self-propelled flapping filaments in tandem configuration. *Phys. Rev. Lett.* **113**, 238105.

ZOU, Q. & HE, X. 1997 On pressure and velocity boundary conditions for the lattice Boltzmann BGK model. *Phys. Fluids* **9** (6), 1591–1598.